ELSEVIER

Chemical Engineering Journal 143 (2008) 51–61

Chemical Engineering Journal

www.elsevier.com/locate/cej

# The simulation of the flow within a hydrocyclone operating with an air core and with an inserted metal rod

Wanwilai Kraipech Evans [a,*], Anotai Suksangpanomrung [b], Andrzej F. Nowakowski [c]

[a] *Department of Chemical Engineering, Srinakarinwirot University, 107 Rungsit-Nakorn-Nayok Road, Ongkharuk, Nakorn-Nayok 26120, Thailand*
[b] *Department of Mechanical Engineering, Academic Division, Chulachomklao Royal Military Academy, Nakorn-Nayok 26001, Thailand*
[c] *Department of Mechanical Engineering, University of Sheffield, Mappin Street, Sheffield S1 3JD, United Kingdom*

Received 20 January 2007; received in revised form 3 September 2007; accepted 9 December 2007

Dedicated to Professor Tomasz Dyakowski who passed away on the 15th of June 2006. He was our colleague, our friend and the driving force behind this research.

**Abstract**

The simulations of the flow within the solid–liquid hydrocyclone operating with an air core and with an inserted metal rod were performed. Finite-volume method and Reynolds stresses model (RSM) were used to model the turbulence characteristic of the flow. The computational results demonstrate the double-vortex flow, which depict the two separation flows. The low-pressure zone or the air core in the centre core was simulated. The redesign hydrocyclone for reducing the energy loss due to this low-pressure core was done by inserting the metal rod in the middle of hydrocyclone. The effect of the inserted-rod on the velocity distributions and the separation performance was investigated. It was found that the separation performance can only be improved with the proper size of the inserted-rod.
© 2007 Elsevier B.V. All rights reserved.

*Keywords:* Hydrocyclone; Computational fluid dynamics; Solid–liquid separation

## 1. Introduction

A hydrocyclone is a piece of separation equipment for solid–liquid and liquid–liquid systems. Recently hydrocyclones have been introduced in the food, oil and textile industries as a result of their simplicity of design and operation, high throughput, low maintenance, low operating cost and small physical size of the unit. Though the consistent use of hydrocyclones has been occuring since the 1950s, the full comprehension of the operation is still ambiguous. As they have many advantages and have been used in many industries, this research work seeks to develop a new approach and improvement in the design and operation of hydrocyclones.

The most popular approach to study the characteristics of hydrocyclones, and consequently to optimize their performance, consists of varying operational parameters, such as pressure drop, cut size, and volumetric throughput and examining the effects of the changes.

Other attempts to model the flow in a hydrocyclone have been made by using the theoretical models, which are based on analytical solution of a set of simplified conservation equations, resulting from mass and momentum conservation principles. Such approach provides a physical insight into the fundamental causes of the observed phenomena. The earlier theoretical models are steady state and 2D-axisymmetrical models, which are limited to dilute flow only. In addition, it is difficult to describe the behaviour of highly turbulent swirling flow caused by the 3D-flow entry. Therefore, more advanced modelling is needed that allows, for example, the study of such phenomena as an adjustment of three-dimensional flow to axisymmetrical, particle–fluid, particle–particle and particle–wall interactions. Such models, which are probably only possible by using computational fluid dynamics, should allow the description of particle effects on suppressing or generating turbulence and non-Newtonian slurry flows. Additionally, in the context of modelling turbulence, a comprehensive physical model is needed to show how a fluid turbulent deformation characterises

* Corresponding author. Tel.: +66 86 999 8908; fax: +66 37 322 608.
*E-mail address:* wanwilai@swu.ac.th (W.K. Evans).

1385-8947/$ – see front matter © 2007 Elsevier B.V. All rights reserved.
doi:10.1016/j.cej.2007.12.023

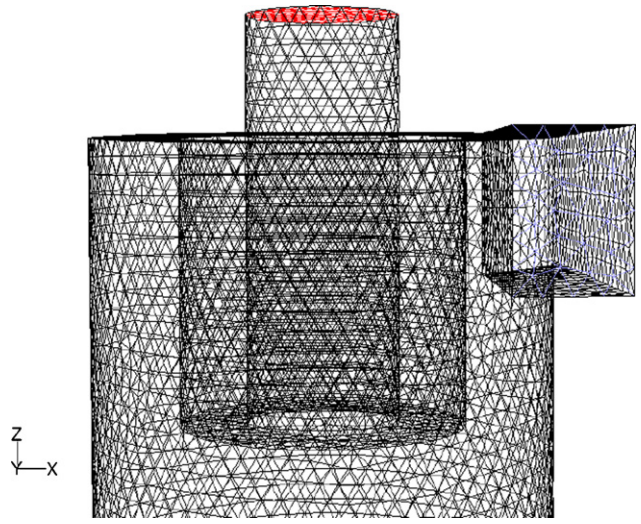


Fig. 1. Unstructured grid consisting of tetrahedral elements within a hydrocyclone for the finite-volume approximation.

swirl flows. Of course, improvements not only in physical modelling but in computational power will need to happen in order for computational modelling to become a viable option [1]. However even with current limitations, computational methods of design have significant advantages over the empirical data, such as freedom of changing the geometry quickly for verification of possible changes in separational efficiency. Furthermore investigation of the embedded turbulence modelling aspects provides a fruitful avenue for understanding a number of open issues regarding internal swirling flow and their implications on separation efficiency of hydrocyclone.

On the other hand, experimentation with changing the internal geometries of a hydrocyclone has been done to try and improve the separational efficiency. Yoshida et al. [2] innovative idea to improve the separational performance was to include a movable guide plate over the inlet.

Other researchers studied the performance of the hydrocyclone operating without an air core. Luo et al. [3] studied the velocity profiles of hydrocyclones by using the laser Doppler anemometry (LDA) technique. They removed the air core by sealing the apex with water and compared the velocity profiles of the ordinary and water-sealed hydrocyclones. They concluded that the water sealed hydrocyclone was superior, but that the capacity was reduced and the seal had to be carefully maintained. Xu et al. [4,5] also measured the velocity components of the hydrocyclone without an air core by using LDA. They replaced the air core with a solid rod and claimed that the air core contributes to the energy loss, and the separation efficiency should increase by removing it. However, they did not validate their statement. In order to test this postulation, Lee and Williams [6] carried out an extensive series of experiments whereby they measured the classification and separation efficiency of the conventional hydrocyclones compared with modified hydrocyclones, in which the air core was replaced by a steel rod insert. They reported that the insertion of a rod into the hydrocyclones does not appear to improve the separation efficiency. In the later, Chu et al. [7] carried out the experiment on the hydrocyclone with an inserted-rod, and they found that the inserted-rod could improve the separation performance of hydrocyclone. They reported that negative effect on the separation found in the experimental study of Lee and Williams [6] might be mainly due to their body supports designed for fixing the solid rod as the main flow field inside the hydrocyclone might be disturbed by the body supports, and the negative effect of this on separation performance might be more remarkable than the positive effect of eliminating the air core. As the result, the hydrocyclone separation performance was not improved, but deteriorated.

The main aim of the present work is to extend this research by introduction of computational fluid dynamics (CFD) techniques to the simulation of 3D flow within a hydrocyclone. This procedure is employed to predict velocity fields in the hydrocyclone with different geometries operating under a wide range

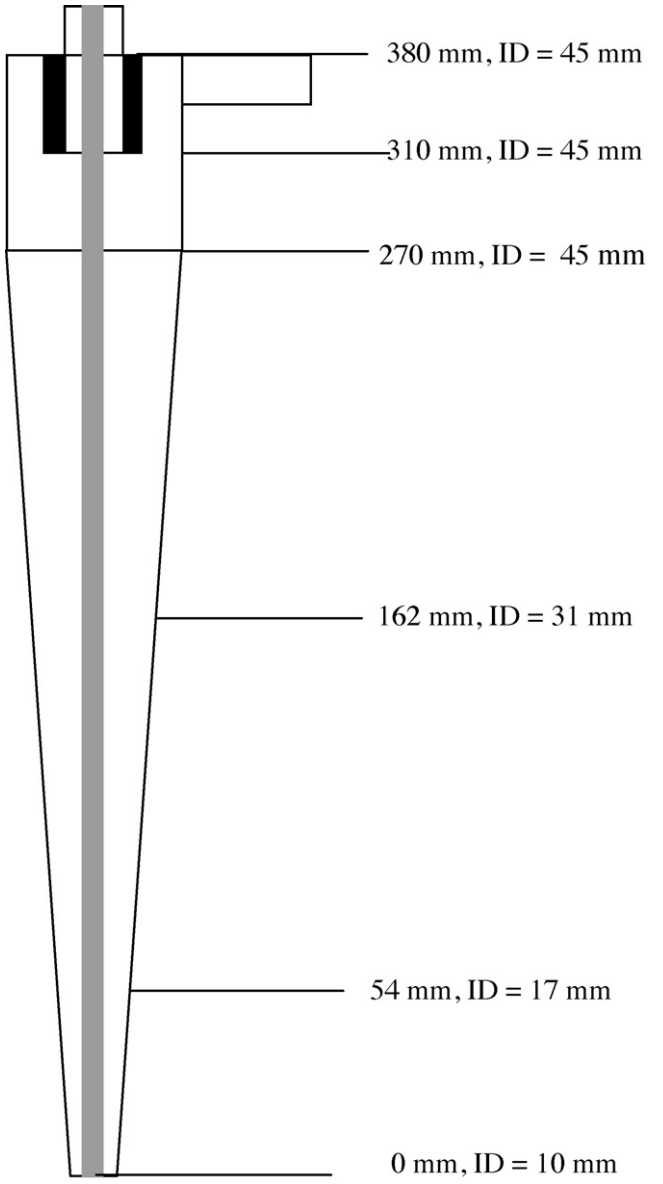


Fig. 2. Schematic diagram shows the plane positions of 50-mm hydrocyclone with inserted-rod. For each plane height the value of the section internal diameter ID is also given.

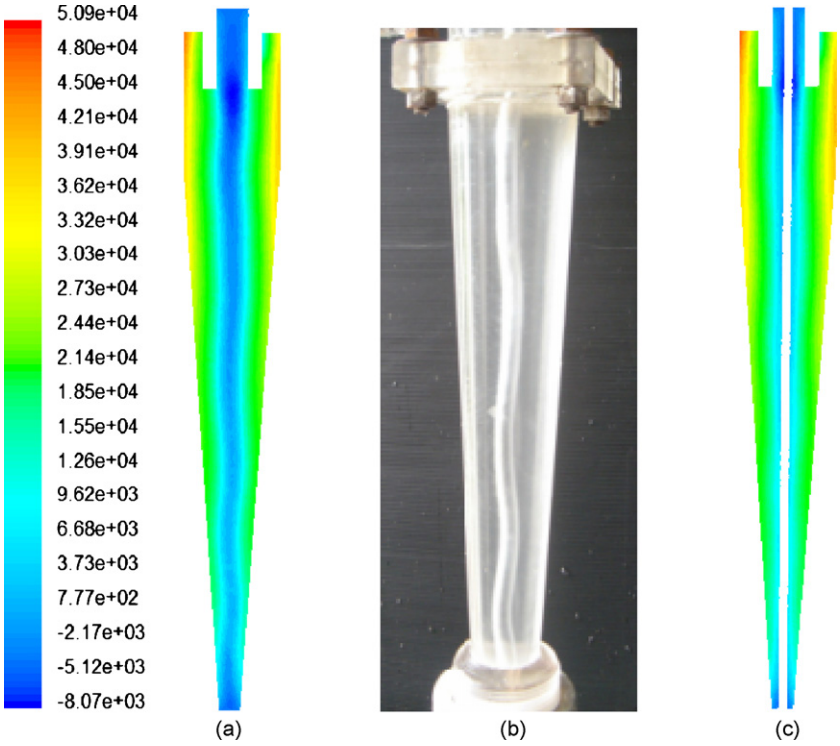


Fig. 3. The obtained pressure (Pa) of fluid projected on a vertical plane of the hydrocyclone: (a) operating with an air core, (b) experimental observation and (c) with 4-mm inserted-rod.

of conditions. A method for predicting particle trajectories in hydrocyclone and its separation efficiency is demonstrated. The numerical results are compared with available experimental data showing good agreement. The flow behaviour and the separation performance of a hydrocyclone operating with an inserted-rod are comparatively studied.

## 2. Problem formulation

### 2.1. Model description and governing equations

The governing partial differential equations are the continuity equation and the Navier–Stokes equations:

$$\frac{\partial \rho}{\partial t} + \rho \frac{\partial \bar{u}_i}{\partial x_i} = 0 \tag{1}$$

$$\frac{\partial(\rho \bar{u}_i)}{\partial t} + \frac{\partial(\rho \bar{u}_i \bar{u}_j)}{\partial x_j} = -\frac{\partial \bar{p}}{\partial x_i} + \frac{\partial}{\partial x_j}\left(\mu \frac{\partial \bar{u}_i}{\partial x_j}\right) + \frac{\partial}{\partial x_j}(-\rho \overline{u_i' u_j'}) + \rho g_i \tag{2}$$

The variables $\rho$, $p$ and $\mu$ represent density, pressure and molecular viscosity, respectively. The velocity $u_i$ is decomposed into its mean and fluctuating components:

$$u_i = \bar{u}_i + u_i' \tag{3}$$

The Reynolds stress term—$\rho \overline{u_i u_j}$ includes the turbulence closure, which is modelled in order to close Eqs. (1) and (2). The recent paper of Delgadillo and Rajamani [8] presents a comparative study of three turbulence-closure models for the hydrocyclone problems. They conclude that Large Eddy simulation (LES) allows the accurate prediction of the velocity profile at different locations. Their simulations demonstrated the dynamics which leads to the formation of the air core. These results were further confirmed by Narasimha et al. [9] in their LES simulations which allowed prediction of air-core diameter and shape. Although LES simulations show considerable potential they are enormously computationally expansive. The subgrid-scale model accounting for the effects of particles has not yet been used in LES simulations. Consequently Reynolds stress model (RSM) has been applied as turbulence closure in this study. The simulations using RSM model and supporting validation studies in the context of hydrocyclones were also presented in recent papers of Bhaskar et al. [10] and Wang and Yu [11]. The RSM model was found to predict well anisotropic turbulence. The RSM provides information of all the stress components and contains exact terms for swirling effects in its stress transport equations. The description of the model is presented in Appendix A.

### 2.2. Modelling particle motion

The motion of particles due to turbulence in the fluid phase was predicted by using the particle trajectory method. The method provides a direct description of the particulate flow by tracking the motion of individual particles. Newton's second law, with semi-empirical forms for the hydrodynamic forces, governs particle motion [12]. The trajectory of the discrete phase particle is obtained by integrating the force balance on the particle. The volume occupied by the particles in a computational cell is

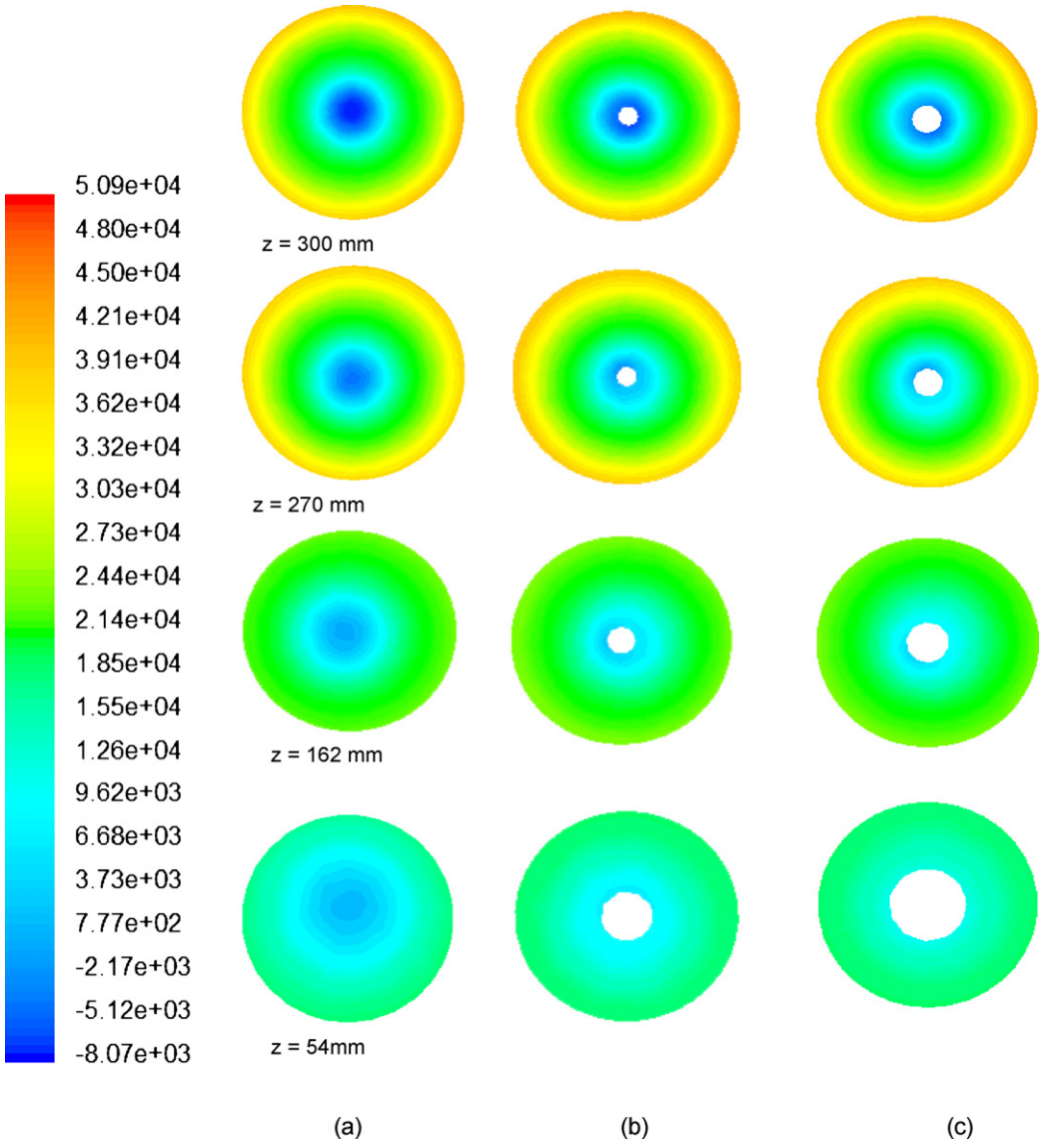


Fig. 4. The obtained pressure (Pa) of fluid projected on a horizontal plane of the hydrocyclone: (a) operating with an air core, (b) with 4-mm inserted-rod and (c) with 6-mm inserted-rod.

neglected. Therefore the particles do not perturb the flow field and the fluid satisfies the continuum equations that are solved on a fixed field. The instantaneous velocity field from the fluid equations is used to predict the trajectories of individual particles. Such coupling mechanism between the phases can only be employed for dilute systems [12]. The particles momentum equations describing a balance between the drag, centrifugal and gravity force are expressed in a Lagrangian reference frame given by

$$\frac{\mathrm{d}v_i}{\mathrm{d}t} = F_\mathrm{D}(u_i - v_i) + \frac{\rho_\mathrm{p} - \rho}{\rho} g_i \tag{4}$$

where $F_\mathrm{D}(u_i - v_i)$ is the drag force per unit particles mass and the relationship for $F_\mathrm{D}$ is

$$F_\mathrm{D} = \frac{18\mu}{\rho_\mathrm{p} d_\mathrm{p}^2} C_\mathrm{D} \frac{Re_\mathrm{p}}{24} \tag{5}$$

Here vector $v_i$ is the particle velocity, $u_i$ is the fluid velocity, $g_i$ is the gravitational acceleration, $C_\mathrm{D}$ is the drag coefficient, $\rho_\mathrm{p}$ is the density of the particle and $d_\mathrm{p}$ is the diameter of the particle. $Re_\mathrm{p}$ is the relative Reynolds number defined as

$$Re = \frac{\rho d_\mathrm{p} |v_i - u_i|}{\mu} \tag{6}$$

### 2.3. Boundary conditions and numerical technique

Since partial differential equations are incorporated in the model, it is necessary to define boundary conditions for all boundaries of the flow domain. At the inlet a uniform velocity boundary condition was applied. For the hydrocyclone configuration studied in this work the simulations were performed for inlet velocities equal to 6, 7 and 8 m/s. For the outlet boundary conditions, the mathematical formulation of the problem does not allow the imposition of fully natural boundary condi-

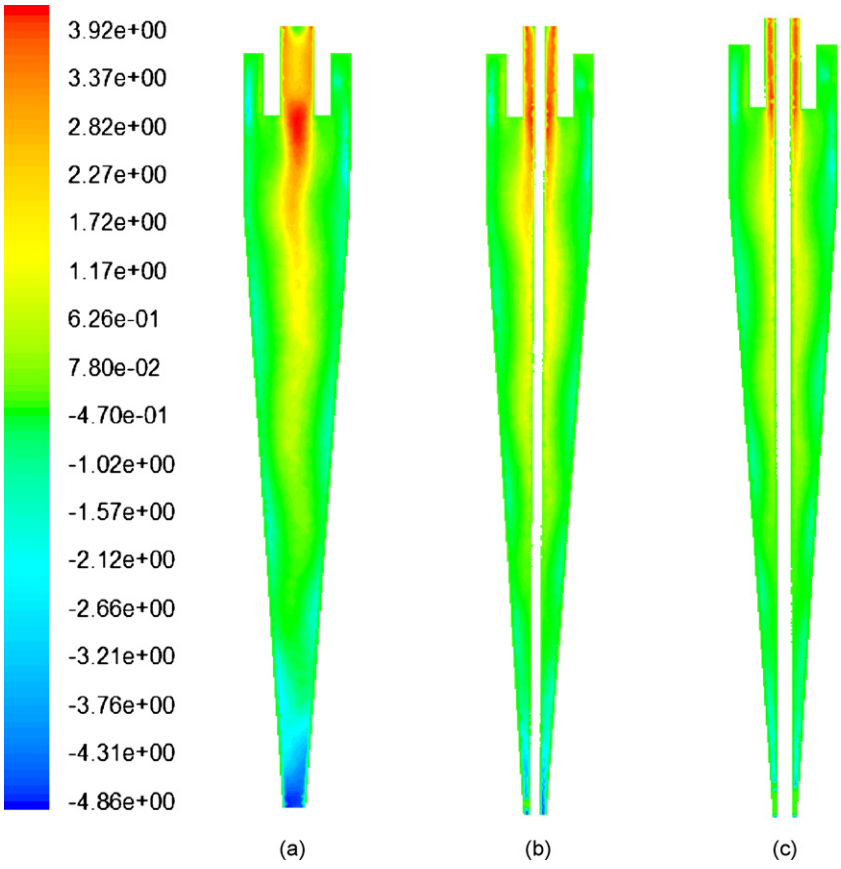


Fig. 5. The obtained axial velocity (m/s) of fluid projected on a vertical plane of the hydrocyclone: (a) operating with an air core, (b) with 4-mm inserted-rod and (c) with 6-mm inserted-rod.

tions in terms of forces as in Doby et al. [13]. Instead pressure boundary conditions, with outlet gauge pressure equal to zero, were applied to the two outlets. This kind of outlet boundary condition was used to simulate the occurrence of the region of negative gauge pressure in the centre of hydrocyclone, which was considered as the air-core zone. The authors also tried to use an interface-tracking algorithm based on the volume of fluid method (VOF) for calculating the position of the air core. However, it was found that the model significantly under-predicted tangential velocities. This confirms observations made by Delgadillo and Rajamani [14] that the RSM model predicts an air core, which is irregular and does not agree with experimental data. No-slip boundary condition is assumed at the solid wall. As a result, all velocity components are zero at the wall. The particles were injected from the feed inlet and left the hydrocyclone through outlet zones.

### 2.4. Numerical scheme

The physical problem was numerically discretized using finite-volume approximation in three-dimensional Cartesian coordinate system. The decoupled solver was chosen for the governing Navier–Stokes equations, which are solved iteratively in sequentional manner until the defined values of convergence are met. The solution method used in this study is the SIMPLEC algorithm developed by Patankar [15]. The continuity and the Navier–Stokes equations are discretized by using QUICK spatial discretization scheme. This is the higher-order scheme allowing for interpolation of field variables from cell centres to faces of the control volumes.

### 2.5. Numerical simulation

The investigation the water flow within a 50-mm hydrocyclone was carried out. The water density and viscosity are 998.2 kg/m$^3$ and $1.003 \times 10^{-3}$ kg/(m s), respectively. The linear systems associated with the solution of the pressure and momentum equations have been solved with a tolerance on the residual to $10^{-6}$. The iterative procedure is declared converged when all residuals have been reduced below $10^{-6}$. The computations were carried out on a PC computer workstation, with FLUENT 6.0 Code and the typical CPU time was 2 days on average for the case with 241,551 computational cells. Grid independence studies were carried out and it was determined that once the number of elements exceeded a value of approximately of 210,000 the solutions of the reported selectivity curves showed a maximum difference of 4.8% between the consecutive grids. This was seen as acceptable; therefore, the final mesh used for all the computations was 241,551 computational cells. The generated unstructured grid consisting of tetrahedral elements is shown in Fig. 1.

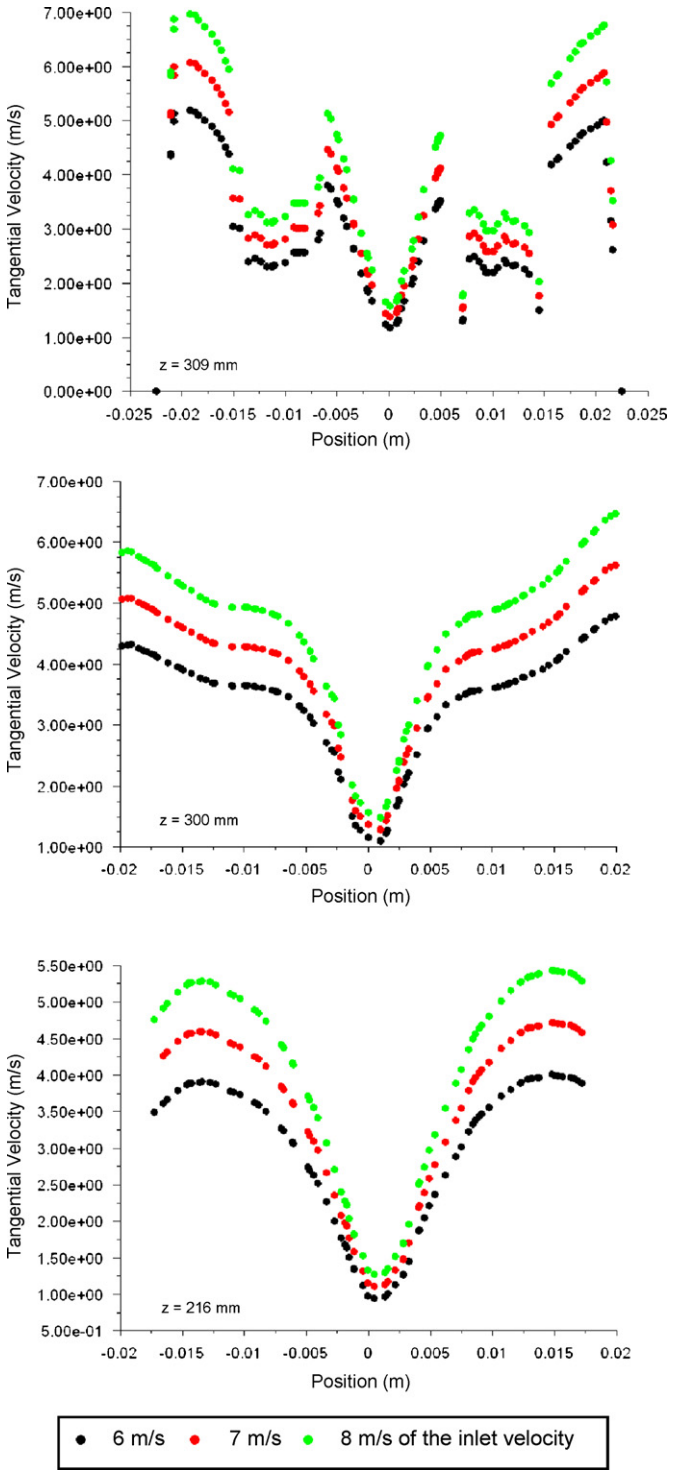


Fig. 6. The tangential velocity profiles (m/s) of fluid on a horizontal plane of the hydrocyclone, operating with an air core, for the inlet velocity of 6, 7 and 8 m/s.

## 3. Numerical results

### 3.1. Flow characteristics

The flow characteristics of the flow within the hydrocyclone are obtained from the post-processing process of the predicted data of the flow pressure and velocity components. The values of the calculated velocities in the Cartesian coordinate system frame are transformed into the tangential, radial and axial velocity components. The schematic diagram shows the plane positions of 50-mm hydrocyclone in Fig. 2.

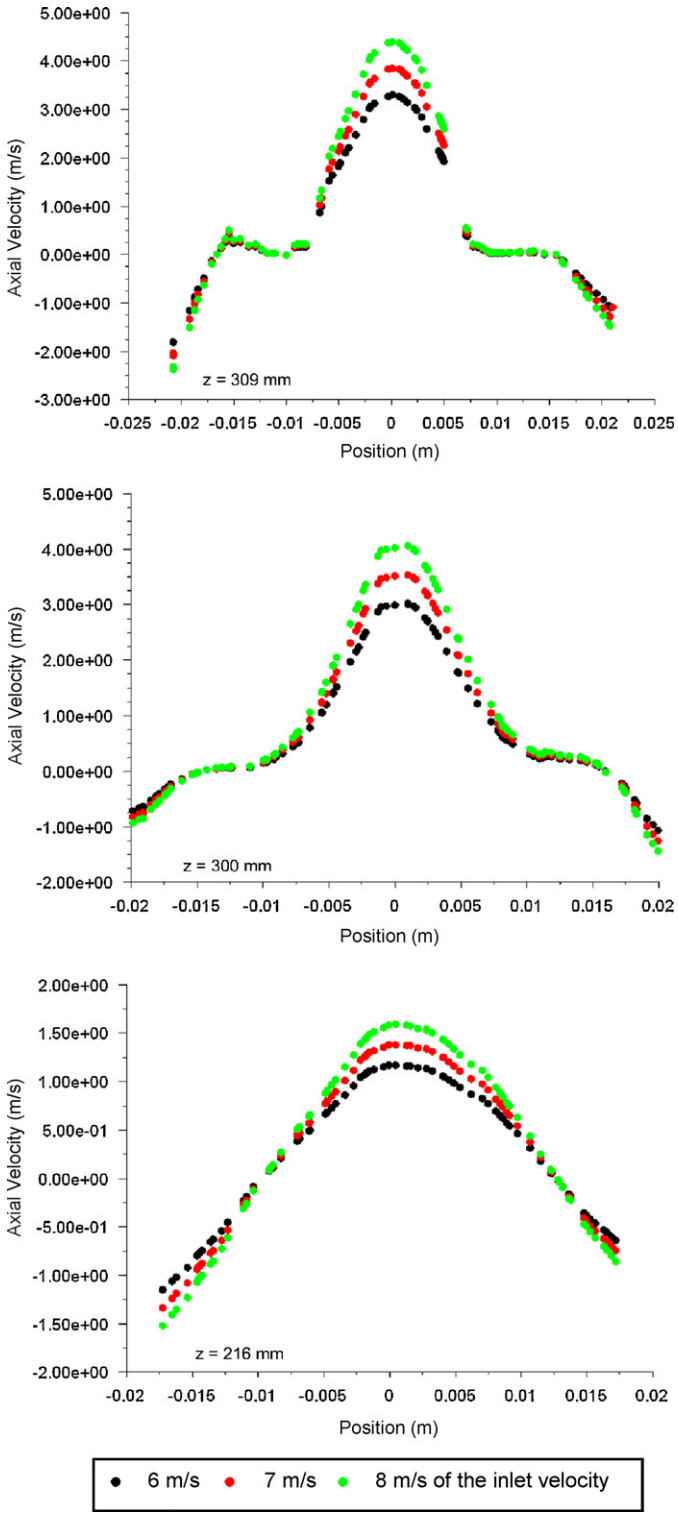


Fig. 7. The axial velocity profiles (m/s) of fluid on a horizontal plane of the hydrocyclone, operating with an air core, for the inlet velocity of 6, 7 and 8 m/s.

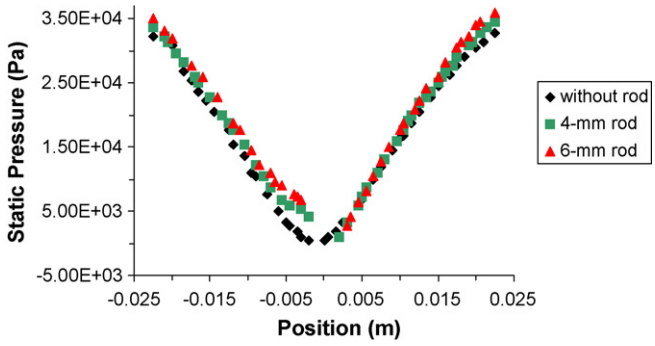


Fig. 8. The profile of static pressure (Pa) of fluid on a horizontal plane at $z = 270$ of the hydrocyclone operating: with 4- and 6-mm rod and without rod.

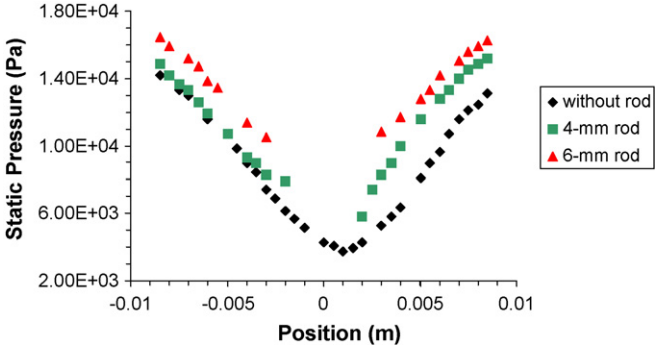


Fig. 9. The profile of static pressure (Pa) of fluid on a horizontal plane at $z = 54$ of the hydrocyclone operating: with 4- and 6-mm rod and without rod.

The obtained pressure of fluid projected on a vertical plane of the hydrocyclone operating with an air core and a 4-mm inserted-rod are shown in Fig. 3. The numerical results can depict the air-core region, where the pressure is negative, in the centre of the hydrocyclone. The air-core characteristics obtained from this numerical simulation is similar to the experimental observation as can be seen in Fig. 3. The air core was found to be instable and its size, shape and position are unfixed because of the instability of the gas–liquid interface. It is also found that the region of the low pressure does not exist in the flow within the hydrocyclone operating with 4-mm inserted-rod. This is due to the inserting of the rod eliminating the occurrence of the air core.

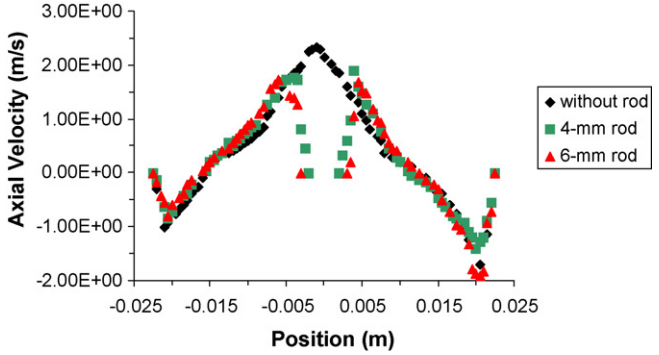


Fig. 10. The profile of axial velocity (m/s) of fluid on a horizontal plane at $z = 270$ of the hydrocyclone operating: with 4- and 6-mm rod and without rod.

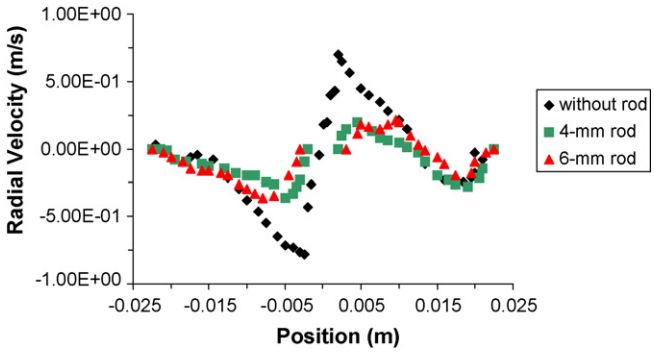


Fig. 11. The profile of radial velocity (m/s) of fluid on a horizontal plane at $z = 270$ of the hydrocyclone operating: with 4- and 6-mm rod and without rod.

The obtained pressure of fluid projected on a horizontal plane of the hydrocyclone operating with an air core, a 4- and 6-mm inserted-rod, are also shown in Fig. 4.

The tangential velocity is an important velocity component as it creates the high swirling field. The fluid enters through the tangential inlet with high inlet velocity and its initially linear motion is converted to angular motion by the hydrocyclone. The numerical result demonstrates a double-vortex pattern or two swirling flows, which are the outer downward and the inner upward flows. It can be seen that the flow within the hydrocyclone is not symmetric.

The separation flow is successfully simulated and can be demonstrated by the axial velocity component as shown in Fig. 5 for both hydrocyclone operating with and without the inserted-rod. The positive and negative values of the axial velocity indicate the upward flow and downward flow, respectively.

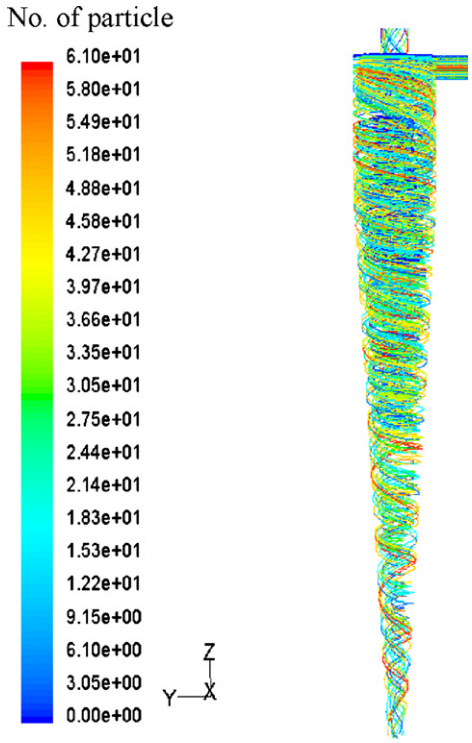


Fig. 12. The trajectory of $CaCO_3$ particles flow within the hydrocyclone operating with air core for the inlet velocity of 7 m/s.

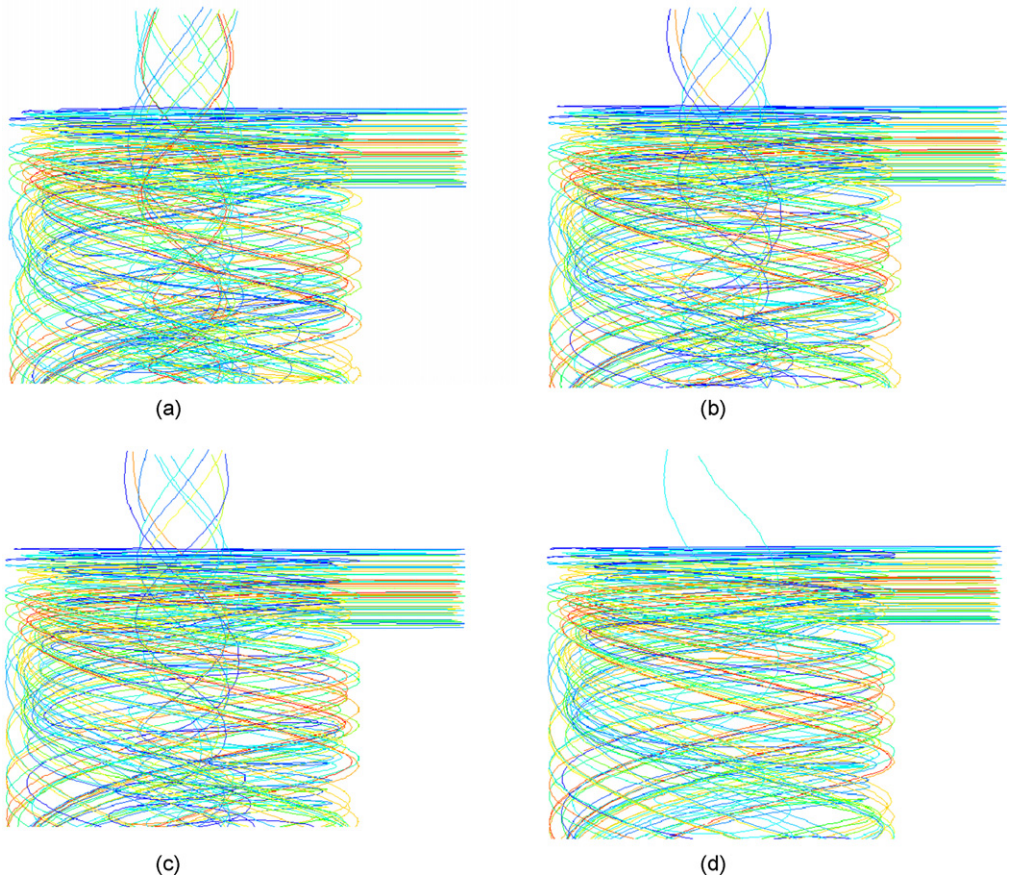


Fig. 13. The trajectory of $CaCO_3$ particles: (a) 1 μm, (b) 2 μm, (c) 5 μm and (d) 10 μm, flow within the hydrocyclone (vortex finder section) for the inlet velocity of 7 m/s.

The inserted-rod causes a lower axial velocity at the underflow outlet area of the separator, because it reduces the underflow outlet area and this causes the reversed upward flow to increase. The typical high axial velocity at the overflow area is observed.

From Figs. 6 and 7, it can be seen that the profiles of both axial and tangential velocity components of the higher inlet velocity case follow the same pattern as that of the lower inlet velocity case. However, the magnitude of both velocity components increases with an increase in the inlet velocity. The axial velocity profiles prove the existence of the LZVV (the location where the zero axial velocity exists), where the separated flow occurs in hydrocyclone. At the plane $z = 309$, which is located in the bottom of the vortex finder tip, the tangential velocity profile is not found to decrease towards the centre like the profile at the plane $z = 300$. This is due to the effect of the upward flow entering the vortex finder tube. The tangential velocity, in the conical section at the plane $z = 216$, tends to increase with decreasing radius until it reaches a maximum at the some point. At radial distances less than this point, the velocity decreases proportionally with the radius. This demonstrates two different zones of forced vortex flow. The tangential velocity profile at the underflow outlet shows the two zones of the swirling flow, while the axial velocity profile demonstrates the reduction of the velocity in the centre caused by the external pressure force.

The pressure is an important parameter of hydrocyclone operation. High-pressure drop in operation means high-energy loss of the flow and high pumping cost. As the result of this numerical simulation, the reduction of pressure loss was found to be reduced by an inserted-rod as shown in Figs. 8 and 9. The hydrocyclone operating without the inserted-rod has lower pressure field that that of the operating with inserted-rod. The 6-mm rod can give the lowest pressure field. This can be seen more clearly at the plane $z = 54$ in Fig. 9.

The axial velocity profile projected on a horizontal plane of the hydrocyclone operating with an air core, a 4- and 6-mm inserted-rod, are shown in Fig. 10.

From the presented numerical result and the experimental data of Chu et al. [7], the upward axial velocity of the fluid in the central area decreased when the air core was replaced by inserted-rod. The decrease of the axial velocity of fluid nearby the entrance of the vortex finder is beneficial to reducing the mixing of coarse particles in overflow product. In Fig. 11, it can be seen that the radial velocity distribution of the flow operating with and without the inserted-rod are similar but the magnitude of the radial velocity of the inserted-rod cases is obviously smaller. The reduction in radial velocity is advantageous for separating fine particles because the drag forces, acting towards the centre, are reduced. The smallest magnitude of the radial veloc-

ity was obtained from the flow with the 4-mm rod, which the best separation performance was found as discussed in the next section.

### 3.2. Particle motion and separation performance

Separation efficiency expresses the relationship between percentages of the each particle size of feed reporting to the underflow discharge. It is commonly used to present the performance of hydrocyclones for particle separation or classification. Its prediction requires a method for tracing particle trajectories as affected by the predicted axial, tangential and redial velocity components. In order to trace the particle trajectory, the particle velocities are obtained from the fluid velocities using the particle momentum Eq. (4) with the drag force per unit particle modelled as (5). The trajectory of a particle depends on the location at which it enters hydrocyclone. Assuming that all particles in the feed stream, despite their difference in size and density, have the same probability of entering the hydrocyclone through any of the entry points, it is possible to determine the trajectory and eventually to compute the particle separation efficiency. The predicted results of particle motions or particle trajectories are shown in Figs. 12 and 13.

In this study, assuming that the particle phase is the particle of $CaCO_3$ within the range of 1–100 μm. All particles are assumed to be spherical. Fig. 12 shows the motions of the particles in a wide range of particle size. The motions of mono-size particle are shown in Fig. 13.

The performance curve, which depicts the percentages of the each particle size of feed reporting to the underflow discharge, is also called the selectivity curve. The selectivity curves for the hydrocyclone operating with an air core for three different inlet velocities are shown in Fig. 14. It was found that the hydrocyclone operate with high inlet velocity can give good separation performance. Since an increase in inlet velocity increases pressure drop and all velocities throughout the hydrocyclone. The pressure drop used in practice usually depends on economic considerations. Operating at high-pressure means less units are required to treat a given flow. The lower capital costs, finer cut sizes and sharper separations can be obtained. These benefits must be offset against drawbacks including higher pumping cost and an increased abrasion. Furthermore, the increase in feed flow-rate and the decrease in cut size tend to decline above a certain pressure drop. This is thought to be due to resistance effects within the hydrocyclone.

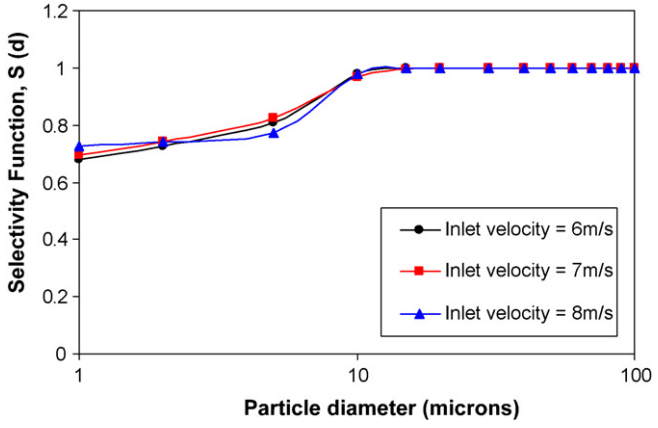


Fig. 14. The selectivity curves, presenting the predicted separation performance, of the flow with an air core for different inlet velocities.

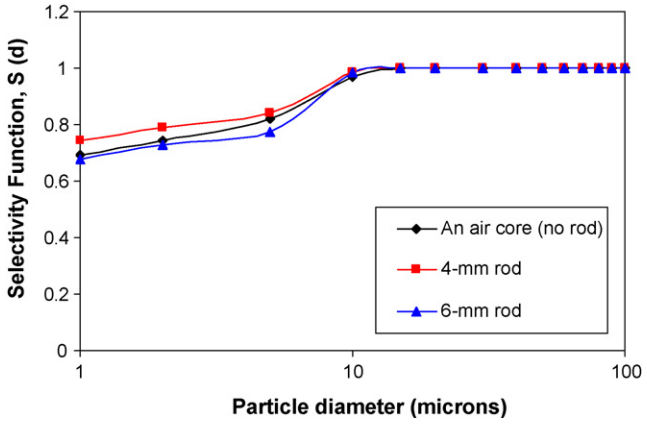


Fig. 15. The selectivity curves, presenting the predicted separation performance, of the flow with an air core (no rod) and 4- and 6-mm inserted rods.

The selectivity curves for the hydrocyclone operating with 4- and 6-mm inserted-rods comparing with that of operating without inserted-rod are presented in Fig. 15. It can be seen that the hydrocyclone operating with the 4-mm inserted-rod gives the best separation performance, while the operating with the 6-mm inserted-rod gives the worst separation performance. These findings were confirmed for different inlet velocities 6, 7 and 8 m/s. It can be concluded that the hydrocyclone separation performance can be improved by replacing the air core with the proper size of the inserted-rod. The negative effect on the separation found in the experimental study of Lee and Williams [6] might be due to both the design of the inserted-rod body supports and the size of inserted-rod.

## 4. Conclusion

The computational fluid dynamics simulations of 3D flow within a hydrocyclone operating with an air core and with inserted-rod by using the finite-volume method have been performed. The particle motion was successfully predicted by using the particle trajectory method. The separation performance of the separator was determined by the relationship between percentages of the each particle size of feed reporting to the underflow discharge. The numerical results from this study were in agreement with the experimental data published earlier. It was found that the radial and axial velocity components in the area just below the vortex finder were reduced, when replacing the air core by inserting a metal rod. This causes the flow field inside hydrocyclone become more beneficial for the separation process. However, the separation performance can only be improved with the proper size of the inserted-rod. The reduction of pressure loss in the hydrocyclone was also found to be reduced by replacing the air core by inserting a metal rod.

**Acknowledgements**

Acknowledgements are due to Mr. Preechanut Panich, Mr. Nitinai Ratchawat, Ms. Pawinee Kongsiri and Ms. Parichat Chanchanaroj for computational and experimental supports and to the Thailand Research Fund for financial support.

## Appendix A

The Reynolds stress model (RSM) is a second-order closure model. The model represents the solution of the transport equations of the six Reynolds stress components together with the equations for the three mean velocities and the dissipation equation for the dissipation rate, $\varepsilon$, of the turbulent kinetic energy. Reynolds stresses are modelled by the following equation:

$$\frac{D(\rho\overline{u_i'u_j'})}{Dt} = \frac{\partial(\rho\overline{u_i'u_j'})}{\partial t} + \frac{\partial\rho u_k\overline{u_i'u_j'}}{\partial x_k} = P_{ij} + D_{T,ij} + D_{L,ij} + \Phi_{ij} + F_{ij} - \varepsilon_{ij} \quad \text{(A1)}$$

The right-hand side terms are

$$P_{ij} = -\rho\left(\overline{u_i'u_k'}\frac{\partial u_j}{\partial x_k} + \overline{u_j'u_k'}\frac{\partial u_i}{\partial x_k}\right) \quad \text{(A2)}$$

$$D_{T,ij} = -\frac{\partial}{\partial x_k}(\overline{p(\delta_{ik}u_j' + \delta_{kj}u_i')} + \rho\overline{u_i'u_j'u_k'}),$$

$$D_{L,ij} = -\frac{\partial}{\partial x_k}\left(\mu\frac{\partial\overline{u_i'u_j'}}{\partial x_k}\right) \quad \text{(A3)}$$

$$\Phi_{ij} = \overline{p\left(\frac{\partial u_i'}{\partial x_j} + \frac{\partial u_j'}{\partial x_i}\right)} \quad \text{(A4)}$$

$$F_{ij} = -\rho\Omega_k(\overline{u_j'u_m'}e_{ikm} + \overline{u_i'u_m'}e_{jkm}) \quad \text{(A5)}$$

$$\varepsilon_{ij} = 2\mu\overline{\frac{\partial u_i'}{\partial x_k}\frac{\partial u_j'}{\partial x_k}} \quad \text{(A6)}$$

The $P_{ij}$ term represents the stress production, $D_{T,ij}$ is the turbulent diffusion term, $D_{L,ij}$ is the molecular diffusion term, $\Phi_{ij}$ is the pressure-strain term, $F_{ij}$ is the pressure-strain term and $\varepsilon_{ij}$ is the rotation production term. Here $\Omega_k$ is the rotation vector, $\delta$ is the Kronecker delta and $e_{ijk} = 1$ if $i$, $j$, $k$ are different and in cyclic order; $e_{ijk} = -1$. if $i$, $j$, $k$ are different and in anti-cyclic order, and $e_{ijk} = 0$ if any two indices are the same.

The dissipation, pressure-strain, and turbulent diffusion terms cannot be computed exactly in terms of the other terms in the equations and therefore are modelled. The pressure-strain term is obtained from a linear-strain model:

$$\Phi_{ij} = \Phi_{ij,1} + \Phi_{ij,2} \quad \text{(A7)}$$

The slow pressure-strain, $\Phi_{ij,1}$ is modelled as

$$\Phi_{ij,1} = -\rho C_1\frac{\varepsilon}{k}\left(\overline{u_i'u_j'} - \frac{1}{3}\overline{u_k'u_k'}\delta_{ij}\right) \quad \text{(A8)}$$

Here, variable $k$ represents the turbulent kinetic energy:

$$k = \frac{1}{2}\rho\overline{u_i'u_i'} \quad \text{(A9)}$$

The rapid pressure-strain term, $\Phi_{ij,2}$ is modelled as

$$\Phi_{ij,2} = -\rho C_2\left(P_{ij} - \frac{1}{3}P_{kk}\delta_{ij}\right) \quad \text{(A10)}$$

The adjustable constants $C_1$ and $C_2$, have the standard values and are equal to 1.8 and 0.6, respectively.The close relation postulated for viscous dissipation term:

$$\varepsilon_{ij} = \frac{\partial}{\partial x_m}\left(C_\mu\frac{k^2}{\varepsilon\sigma_\varepsilon}\frac{\partial\varepsilon_{ij}}{\partial x_m}\right) + C_{1\varepsilon}C_\mu E_{ij}E_{ij} - C_{2\varepsilon}\frac{\varepsilon^2}{k} \quad \text{(A11)}$$

The adjustable constants $C_\mu, C_{1\varepsilon}, C_{2\varepsilon}, \sigma_k, \sigma_\varepsilon$ are 0.09, 1.44, 1.92, 1.0 and 1.3, respectively. The mean strain rate is $E_{ij}$ expressed as

$$E_{ij} = \frac{1}{2}\left(\frac{\partial u_i}{\partial x_j} + \frac{\partial u_j}{\partial x_i}\right) \quad \text{(A12)}$$

In the near-wall region of hydrocyclones the solution variables change with large gradients. The popular near wall models (wall functions) do not resolve accurately the near-wall region for strongly swirling flows. Due to the significant stream-wise pressure gradients, body forces and strong secondary flows the assumption of local equilibrium does not hold. Therefore the fluent two-layer zonal model was found to be more suitable. The two-layer near wall models divide the whole domain into two regions, a viscosity affected region and a fully turbulent region. The demarcation of the two region is determined by a wall distance-based, turbulent Reynolds number:

$$Re_y = \rho y\frac{\sqrt{k}}{\mu} \quad \text{(A13)}$$

where $y$ is the normal distance from the wall at the cell centres. In the near-wall region when $Re_y < 200$, the one-equation model of Wolfstein [16] is employed. For the values $Re_y > 200$ the RSM model is used.

## References

[1] A.F. Nowakowski, J.C. Cullivan, R.A. Williams, T. Dyakowski, Application of CFD to modeling the flow in hydrocyclones is this a realizable option or still a research challenge? Miner. Eng. 17 (2004) 661–669.
[2] H. Yoshida, T. Takashina, K. Fukui, T. Iwanaga, Effect of inlet shape and slurry temperature on the classification performance of hydrocyclones, Powder Technol. 140 (2004) 1–9.
[3] Q. Luo, C. Deng, J.R. Xu, L. Yu, G. Xiong, Comparison of the performance of the water sealed and commercial hydrocyclones, Int. J. Miner. Process. 25 (1989) 297–310.
[4] J. Xu, Q. Luo, J. Qiu, Studying the flow field in a hydrocyclone with no forced vortex. Part I. Average velocity, Filtr. Sep. 27 (1990) 181–182.
[5] J. Xu, Q. Luo, J. Qiu, Studying the flow field in a hydrocyclone with no forced vortex. Part II. Average velocity, Filtr. Sep. 27 (1990) 356–359.
[6] M.S. Lee, R.A. Williams, Performance characteristics within a modified hydrocyclones, Miner. Eng. 6 (1993) 743–751.
[7] L. Chu, W. Yu, G. Wang, X. Zhou, W. Chen, G. Dai, Enhancement of hydrocyclone separation performance by eliminating the air core, Chem. Eng. Process. 43 (2004) 1441–1448.

[8] J.A. Delgadillo, R.K. Rajamani, A comparative study of three turbulence-closure models for the hydrocyclone problem, Int. J. Miner. Process. 77 (2005) 217–230.
[9] M. Narasimha, M. Brennan, P.N. Holtham, Large eddy simulation of hydrocyclone—prediction of air-core diameter and shape, Int. J. Miner. Process. 80 (2006) 1–14.
[10] K.U. Bhaskar, Y.R. Murthy, M.R. Raju, S. Tivari, J.K. Srivastava, N. Ramakrishnan, CFD simulation and experimental validation studies on hydrocyclone, Miner. Eng. 20 (2007) 60–71.
[11] B. Wang, A.B. Yu, Numerical study of particle–fluid flow in hydrocyclones with different body dimensions, Miner. Eng. 19 (2006) 1022–1033.
[12] W. Kraipech, A.F. Nowakowski, T. Dyakowski, A. Suksangpanomrung, An investigation of the effect of the particle–fluid and particle–particle interactions on the flow within a hydrocyclone, Chem. Eng. J. 111 (2005) 189–197.
[13] M.J. Doby, W. Kraipech, A.F. Nowakowski, Numerical prediction of outlet velocity patterns in solid–liquid separators, Chem. Eng. J. 111 (2005) 173–180.
[14] J.A. Delgadillo, R.K. Rajamani, Exploration of hydrocyclone designs using computational fluid dynamics, Int. J. Miner. Process. 84 (1–4) (2007) 252–261.
[15] S.V. Patankar, Numerical Heat Transfer and Fluid Flow, Hemisphere Publishing Corporation, Taylor and Francis Group, New York, 1980.
[16] M. Wolfstein, The velocity and temperature distribution of one-dimensional flow with turbulence augmentation and pressure gradient, Int. J. Heat Mass Transfer 12 (1969) 301–318.